International Journal of Heat and Mass Transfer 217 (2023) 124709

Contents lists available at ScienceDirect

International Journal of Heat and Mass Transfer

journal homepage: www.elsevier.com/locate/ijhmt

Experimental investigation of the heat transport and pressure drop in open-cell polyurethane foams

Aidar Hayrullin *, Alex Sinyavin, Aigul Haibullina, Vladimir Ilyin

Faculty of Thermal Power Engineering, Kazan State Power Engineering University, 51 Krasnoselskaya Street, 420066 Kazan, Russia

ARTICLE INFO

Keywords:
Polyurethane foam
Open-cell foam
Heat transfer
Pressure drop

ABSTRACT

Foam-like materials have a large specific surface area and complex structure that promotes flow turbulence, which makes them useful for heat transfer. In the literature, heat transfer in metal foams (MF) with high thermal conductivity is mainly considered. In the present paper, an experimental study of the hydraulic and heat transfer characteristics of a rectangular channel filled with polyurethane foam (PUF) inserts with a thermal conductivity of 0.2 $W{\cdot}m^{-1}{\cdot}K^{-1}$ in the air flow was carried out. The open-cell PUF samples had 20 and 80 pores per inch (PPI), 0.97 and 0.98 porosity, 269 μm and 60 μm fiber diameter, respectively. The Reynolds number, based on the fiber diameter ranged from 0.04 to 50. From the results of hydraulic tests, friction coefficients were determined based on the fiber diameter and permeability. The Forchheimer coefficient was 0.198 and 0.318 for 20 and 80 PPI samples, respectively. The permeability was 1.889 $10^{-7}\ {\cdot}m^2$ and 7.535 $10^{-9}\ {\cdot}m^2$ for 20 and 80 PPI samples, respectively. The Nusselt number for both tested PUF samples was correlated with the Reynolds number based on the fiber diameter in a power law with the Reynolds number exponent and constant equal to 0.61 and 0.037 respectively. The intensity of heat transfer in the PUF samples was 7–12 times lower than that in MF. However, a significant heat transfer enhancement is still possible compared to the empty channel up to 7 times. The heat transfer performance of PUF was higher compared to the empty channel, but the thermal performance factor was lower than one. Nevertheless, in practical situations where the mass or cost of the heat exchanger is preferable, PUF can be considered as a heat transfer intensifier.

1. Introduction

The use of efficient compact heat exchangers is essential in many engineering applications. Highly porous open-cell foams are widely used in various engineering applications such as heat sinks [1], heat exchangers [2], fuel-cell stacks [3], heat pipe systems [4], heat storage [5], catalytic reactors [6] and thermoelectric generators [7]. The porous structures of open-cell foams increase heat transfer because of a high specific surface area and a complex three-dimensional structure. Porous open-cell foams are made from materials with high thermal conductivity, which allows for a further increase in the heat transfer [8].

Mancin et al. [9] presented the results of an experimental study of heat transfer in seven aluminum foam samples with different pore per inch (PPI) and porosity. As a result, they developed a scheme for overall heat transfer coefficient (HTC) calculations. Additionally, an empirical correlation was proposed to predict the interstitial heat transfer coefficient in the foam as a function of the Reynolds number based on the fiber diameter. Furthermore, Mancin et al. [10,11] experimentally studied the heat transfer of aluminum foam with different (PPI) and heights, using air as the working fluid. The results showed that samples with a height of 20 mm had a higher HTC than those with a height of 40 mm. In another study, Mancin et al. [12] studied twenty-one aluminum and copper foam samples with different PPI and porosities. It was shown that the overall HTC of the copper foam at the same mass velocities was superior to that of aluminum. Durmus et al. [13] studied open-cell aluminum foams with different ratios of large and small pores. Foams with 67% large pores and 33% fine pores exhibited the most attractive heat characteristics at the lowest pressure drop. Sun et al. [14] experimentally investigated heat transfer properties of different NiCr foams and one Kevin cells manufactured with additive technology. The results of the study showed that overall HTC of Kelvin cells can be higher than NiCr foams up to 64.4%. Calmidi and Mahajan [15] the presented results of an experimental and numerical study of forced air convection through MF with porosity ranged from 0.89 to 0.97 and PPI varied from 5 to 40. The Nusselt number data were presented as a function of the permeability based Reynolds number. An empirical correlation was also proposed for predicting the interstitial heat transfer coefficient obtained

* Corresponding author.
E-mail address: kharullin@yandex.ru (A. Hayrullin).

https://doi.org/10.1016/j.ijheatmasstransfer.2023.124709
Received 22 May 2023; Received in revised form 1 September 2023; Accepted 13 September 2023
Available online 17 September 2023

Abbreviations

A	coefficient in Eq. (5) [–]
A_{wall}	area of the aluminum heated wall
B	coefficient in Eq. (5) [–]
b_1	coefficient in Eq. (1) [–]
b_2	coefficient in Eq. (1) [–]
c_p	air heat capacity J kg^{-1} K^{-1}
d_f	fiber diameter [m]
E	emissivity [–]
E_0	emissivity configured in the thermal imager [–]
F	Forchheimer coefficient [–]
G	air mass velocity [kg m^{-2} s^{-1}]
f_{d_f}	friction factor based on the fiber diameter [–]
f_D	friction factor based on the hydraulic diameter with PUF inserts [–]
f_D^0	friction factor of the empty channel [–]
f_K	friction factor based on the permeability [–]
HTC	overall heat transfer coefficient [W m^{-2} K^{-1}]
j	Colburn factor [–]
K	permeability [m^2]
k_f	flow thermal conductivity [W m K^{-1}]
k_s	solid thermal conductivity [W m K^{-1}]
$\dot{m}$	air mass flow rate [m s^{-1}]
Nu_D	Nusselt number Nu_D based on a channel hydraulic diameter with PUF inserts
Nu_D^0	Nusselt number of the empty channel [–]
Nu_{d_f}	Nusselt number based on the fiber diameter [–]
Nu_K	Nusselt number based on the permeability [–]
PPI	Pores number per linear inch [pores in^{-1}]
Pr	Prandtl number [–]
Q	heat flow rate [W]
Re_{d_f}	Reynolds number based on the fiber diameter [–]
Re_K	Reynolds number based on the permeability [–]
St	Stanton number [–]
T_{flow}	flow temperature [°C]
T_{inlet}	inlet temperature [°C]
T_{outlet}	outlet temperature [°C]
t_{TI}	temperature measured by the thermal imager [°C]
t_{TC}	temperature measured by the thermocouple [°C]
T_{wall}	wall temperature [°C]
u	average velocity in the PUF [m s^{-1}]
u_o	average velocity in the channel [m s^{-1}]

Greek symbols

$\Delta P/L$	pressure gradient [Pa m^{-1}]
ΔT	mean temperature difference [K]
ε	porosity [–]
μ	dynamic viscosity [Pa s]
ρ	air density [kg m^3]

Abbreviation

MF	metal foam
PUF	polyurethane foam
TPF	thermal performance factor

from numerical and experimental studies. Kouidri and Madani [16] experimentally studied forced convection through MF with different effective thermal conductivity. Based on the results of an experimental study, an empirical correlation was proposed that, in addition to the Reynolds and Prandtl numbers, also includes the effective thermal conductivity ratio. The results showed that, at the same mass velocities, the material with the highest effective thermal conductivity had the highest overall HTC.

Hamadouche et al. [17] investigated the heat transfer of open-cell aluminum foam with an air velocity from 1 to 5 m s^{-1}. The results showed a 300% increase in heat transfer compared with an empty channel. The heat transfer characteristics of flow through an aluminum foam channel have been investigated by Hwang et al. [18]. The Reynolds number was based on the pore diameter. It was shown that at a fixed Reynolds number, the heat transfer of the aluminum foam decreased with increasing porosity. Noh et al. [19] experimentally investigated the heat transfer during flow in an annulus with a highly porous aluminum foam insert. The results showed that aluminum foam increased the heat transfer from the surface compared with laminar flow in an empty annulus. A correlation for the Nusselt number is proposed. The intensification of the heat transfer during forced convection in a channel with foam metal inserts was studied experimentally by Hutter et al. [20]. Compared with an empty tube, foam metal inserts resulted in up to 10 times more heat transfer. It is shown that with fully sintered foam with a tube wall, the heat transfer is higher on average by 30% compared to foam without a connection to the wall. Huang et al. [21] studied the thermal performance of tube with porous media inserts made by copper screens. The heat transfer enhancement of the tube with copper screens inserts increased by a factor of 5.5 compare with the empty tube in laminar flow. The experimental results showed that the heat transfer rate under constant pumping power with porous media inserts exceeded that of the empty tube by a factor of 1.44. Arbak and Dukhan [22] experimentally studied the thermal performance of MF filled rectangular channel, with 20 PPI aluminum foam. It is shown that the Colburn j factor for MF was higher than an empty channel by 407%.

Dietrich [23] presented experimental results of the ceramic sponges heat transfer with different porosity and pore size. The overall HTC of the ceramic sponges increased from

40 to 500 W m^{-2} K^{-1} with an increase in the superficial air velocity from 0.5 to 5 m s^{-1}. Xu et al. [24] investigated the convective heat transfer for ceramic foam. It is shown that the thickness of sample had a significant effect on the volumetric heat transfer. Based on the experimental results, a new correlation was proposed that includes the porosity, thickness of the sample, superficial velocity and fluid properties.

Dukhan and Patel [25] investigated the pressure drops in MF with different porosities and PPI. They proposed an empirical model for the pressure drop in MF using easily measurable parameters. It concluded that the reciprocal of the surface area density can be used as the length scale for pressure drop prediction using a new definition of the kinetic friction factor. Dietrich et al. [26] experimentally measured the pressure drop in ceramic sponges with different PPI and porosity. The authors concluded that the pressure drop of sponges can be predicted using an Ergun-type equation, with two predefined constants of the Ergun equation from the experimental data. Paek et al. [27] presented the results of experimental measurements of the permeability and pressure drop of aluminum-based MF. It has been shown that at a fixed porosity, with an increase in the cell size, the permeability increases. According to the results of experimental studies, an empirical correlation for the friction fraction prediction was developed. Wang and Guo [28] studied the pressure drop through stainless steel foam at a porosity of 0.93, PPI of 10, 30 and 70 and with relatively high air flow velocities ranged from 7.0 to 26.0 m s^{-1}. According to experimental studies, a new correlation for the pressure drop through MF was presented.

The overall HTC in a porous medium is transferred by the thermal conductivity of the solid material and the interfacial convective heat

Table 1
Characteristics of the tested foams.

Sample code	Porosity	Fiber diameter, d_f (um)	PPI	Thermal conductivity of solid phase at room temperature, k_s ($W \cdot m^{-1} \cdot K^{-1}$) [34,35]	Specific heat of solid phase ($J \cdot kg^{-1} \cdot K^{-1}$) [36]	Density of solid phase, ($kg \cdot m^{-3}$) [36]
PUF-20	0.97	269±8(0.95)	20	0.2	2000	800–1025
PUF-80	0.98	60±3(0.95)	80	0.2	2000	1917–2000

transfer coefficient between the solid material and flow. For better heat transfer in solid materials, foams are often made of materials with high thermal conductivities aluminum and copper. When air is used as the working fluid, the solid thermal conductivity of the MF can exceed the thermal conductivity of the fluid by three to four orders of magnitude. Because air has low thermal conductivity, heat transfer in a porous medium is determined by the thermal conductivity of a solid material. The higher the thermal conductivity of the material, the higher the overall HTC of the porous medium. Wang and Guo [29] investigated heat transfer in MF using the local thermal non-equilibrium model. They demonstrated that with an increase in the thermal conductivity coefficient of the material k_s to 150 $W \cdot m^{-1} \cdot K^{-1}$, a significant increase in the volumetric convective heat transfer coefficient of the MF occurred. When the thermal conductivity of the material was higher than 150 $W \cdot m^{-1} \cdot K^{-1}$, the volumetric convective heat transfer coefficient had a small change. Lu et al. [30] studied the overall HTC in MF filled pipes analytically using the two-equation heat transfer model and Brinkman-extended Darcy momentum model. It showed that the overall HTC of the MF increased significantly with increasing solid thermal conductivity of MF. The overall HTC increased with increasing PPI and decreased with increasing porosity, which was more pronounced at a higher solid thermal conductivity of MF. Xu et al. [31] presented the results of numerically investigation of the overall HTC in MF using the local thermal equilibrium model and the local thermal non-equilibrium model. The thermal conductivity ratios of the fluid and solid ranged from 10^{-6} to 1. For the local thermal equilibrium model and the local thermal non-equilibrium model, when the thermal conductivity ratio changed from 10^{-6} to 1, the overall HTC changed by four orders and two orders, respectively. Edouard et al. [32] experimentally studied the overall HTC in polyurethane foam PUF. The results showed that although the flow rate varied from 0.018 to 0.32 m s^{-1}, the overall HTC averaged 110 W m^{-2} K^{-1} ± 15%, so correlation for overall HTC was impossible. Kaviany and Mittal [33] studied the pressure drop in the PUF for different PPI and the porosity of 0.98 with natural convection from a vertical plate placed next to the PUF. For all studied PUF, the permeability and Forchheimer coefficients were obtained.

In most studies, the heat transfer characteristics of open-cell foams with high thermal conductivities, such as copper and aluminum foams, have been investigated. There is a lack of experimental data on forced convective heat transfer in foams with low thermal conductivity. The thermal conductivity of MF solid phase is essential for the overall HTC, especially for air flow. The main aim of this study was to present the results of the overall HTC and friction factor of two PUF with a thermal conductivity of the solid phase k_s of 0.2 $W \cdot m^{-1} \cdot K^{-1}$, and porosity of 0.97 and 0.98. Nevertheless, it is evident that the HTC of foams with low thermal conductivity is lower than that of MF. However, it cannot be simply evaluated from the HTC of MF. In addition, the heat transfer and hydraulic characteristics of PUF have been poorly studied. The thermodynamic characteristics of the PUF are different from those of MF, not only because of the low thermal conductivity, but also because of higher porosity, ligament surface, etc. Additionally, the aim of this study was to investigate which characteristic length is more suitable for the Nusselt number and friction factor correlation. Furthermore, considering the mass and cost of PUF, it can be used for heat transfer enhancement.

2. Experimental setup and measurement procedure

The heat transfer characteristics and pressure drop were studied for the two PUF. The characteristics of the tested foams are presented in Table 1. The numbers of PPI and fiber diameter were determined using an analog microscope. In six different places on each foam sample, five fiber diameters were measured using a microscope and an optical micrometer with a resolution of 10 μm. The magnifying power of the microscope was 8, thus the overall uncertainty of the fiber diameter measurement was no more than 10/8 μm. After measuring at least 30 separate fibers, the final uncertainties in the fiber diameters were defined as 2.96% for PUF-20 and 4.5% for PUF-80. Fig. 1 shows the structure of tested foams and an 8x magnified image of fibers. The dimensions of all the tested samples were 105 × 55 × 200 mm (width, height and length).

For the convective heat transfer analysis, the tested samples were placed in an air test channel (Fig. 2). The test channel was a rectangular plastic tube with dimensions of 107 × 52 mm and 20-mm-thick insulated polystyrene foam shells, and the total length of the channel was 920 mm. An aluminum plate (120 mm by 80 mm) was inserted for the heat source in the top wall, and a cut in the insulation (heated window) was made. Without any air gaps, the foam test sample was firmly inserted into the channel beneath the heated plate. To obtain a uniform velocity field in the heat transfer zone, stabilization sections were provided before (length: 340 mm) and after (length: 190 mm) the sample. In order to measure the mass-flow-averaged temperature of the heated air, a mixer was installed at the outlet section of the channel, and a 25 mm diameter round perforation was used for the outlet.

A diagram of the test rig is shown in Fig. 3. Air was supplied with a

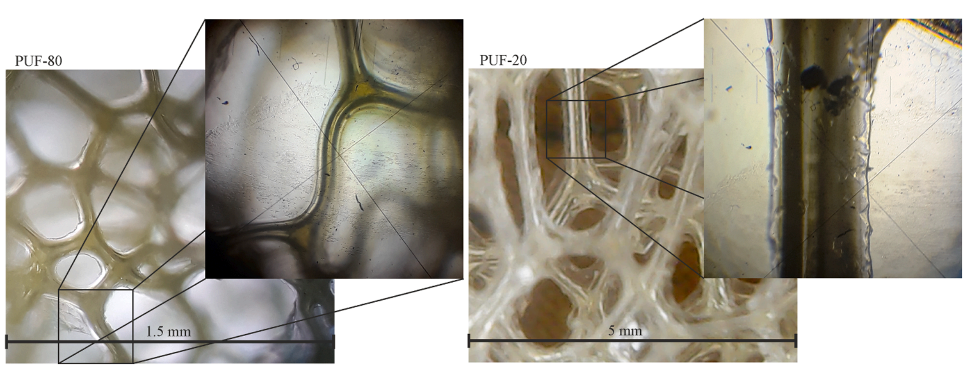

Fig. 1. Tested foam's photos taken by the analog microscope.

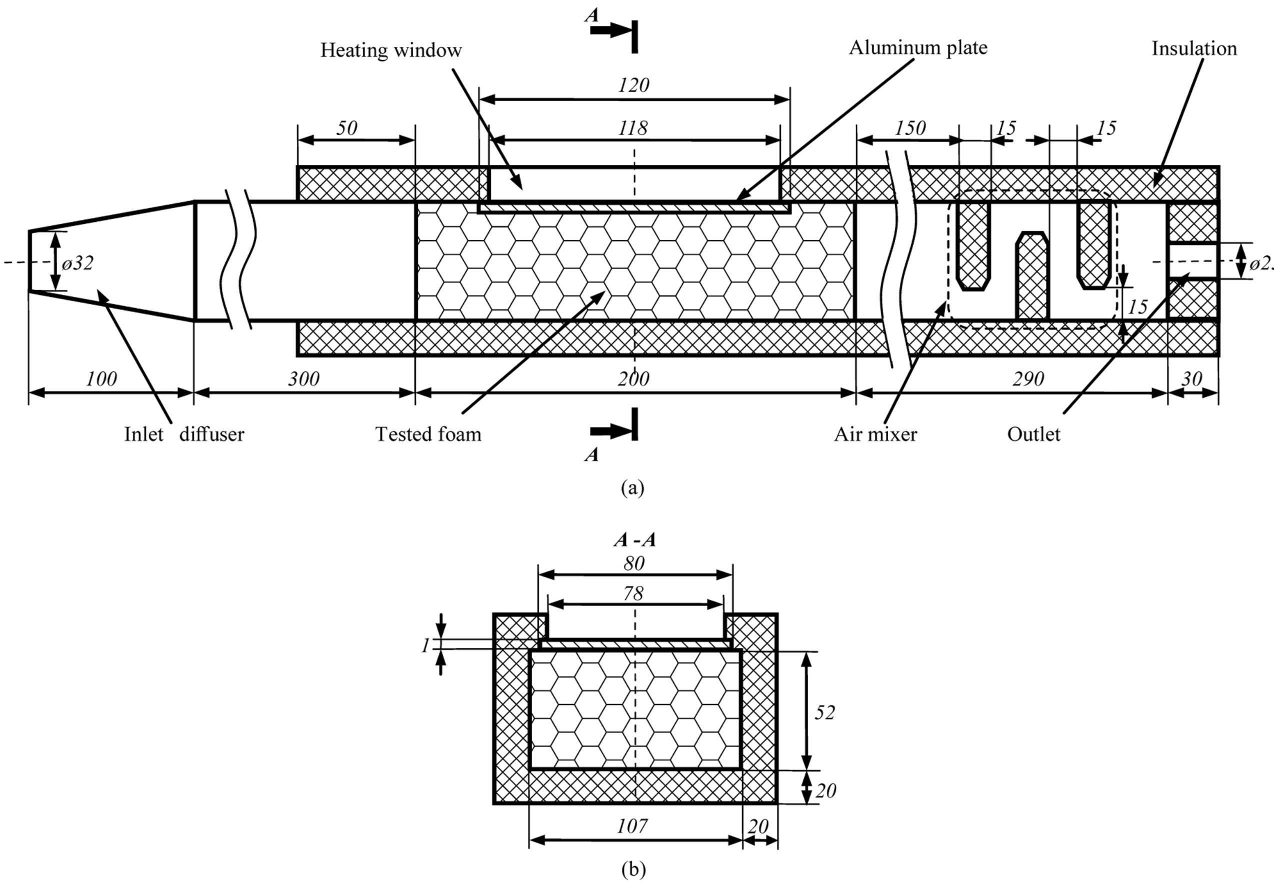

Fig. 2. Test section (lengths are in mm): (a) side view (section view); (b) front view (section A-A).

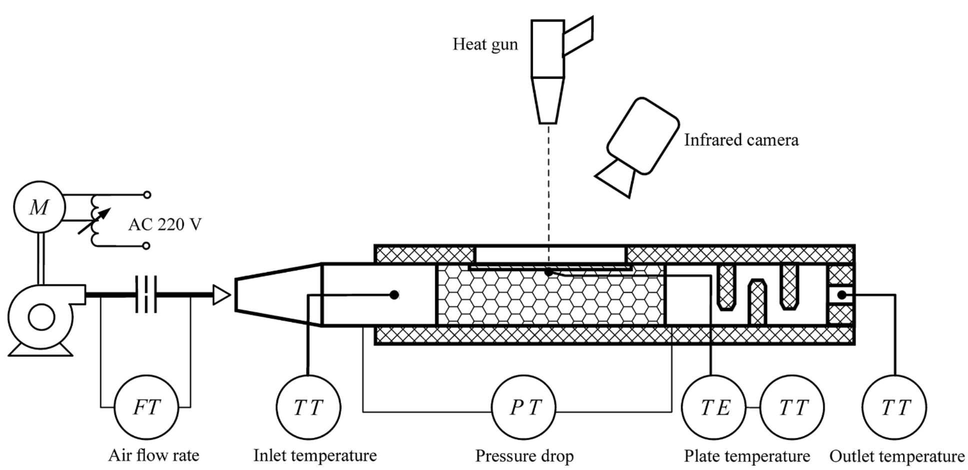

Fig. 3. The diagram of the experimental setup.

centrifugal blower (the maximum flow rate was 100 m^3 h^{-1} and the maximum pressure was 10 kPa). The flow rate is regulated using an automatic transformer. To measure it, an orifice plate and the differential pressure transducer Proma-IDM-DD-6 with a range of 0–6 kPa and an accuracy of ±0.5% were used. To heat the aluminum plate, a hot air jet from a heat gun (whose maximum power was 1.5 kWt and whose maximum temperature was 300 °C) was used. To achieve the necessary temperature of the plate, a distance between it and the heat gun should be adjusted. The air temperatures before the test sample and at the channel outlet were measured with the temperature transducers Relsib DWT-02, which had a range of –40 to +85 °C and an accuracy of 1.0 °C. To increase reliability, a K-type thermocouple with an accuracy of 1.0 °C was recessed in the middle of the plate's back side.

Before the experiment, the temperature transducers and thermocouple were calibrated for a temperature range of +25 to +85 °C using a heat bath and a precise platinum RTD with an accuracy of 0.01 °C [37, 38]. The calibration decreased the uncertainty of DWT transducers to ±0.03 °C and for the thermocouple to ±0.2 °C.

The pressure drop was also measured using the differential pressure sensor PROMA-IDM-DD-6 connected to the channel at the inlet and outlet of the tested foam. Data from transducers was recorded with a data acquisition system on a laptop (not shown in the Fig. 3).

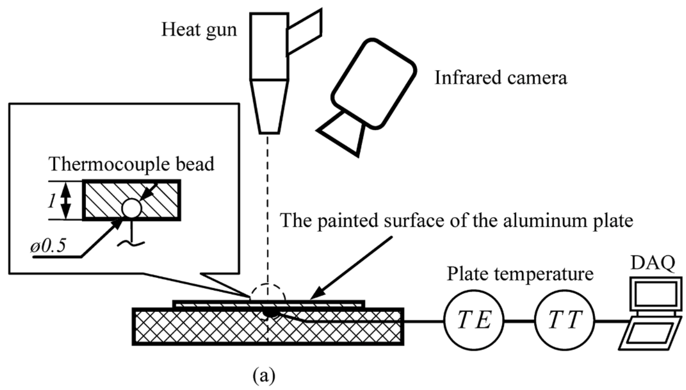

Fig. 4. The thermo imager calibration setup (lengths are in mm): (a) the diagram of the experimental setup; (b) the aluminum plate top view with dimensions.

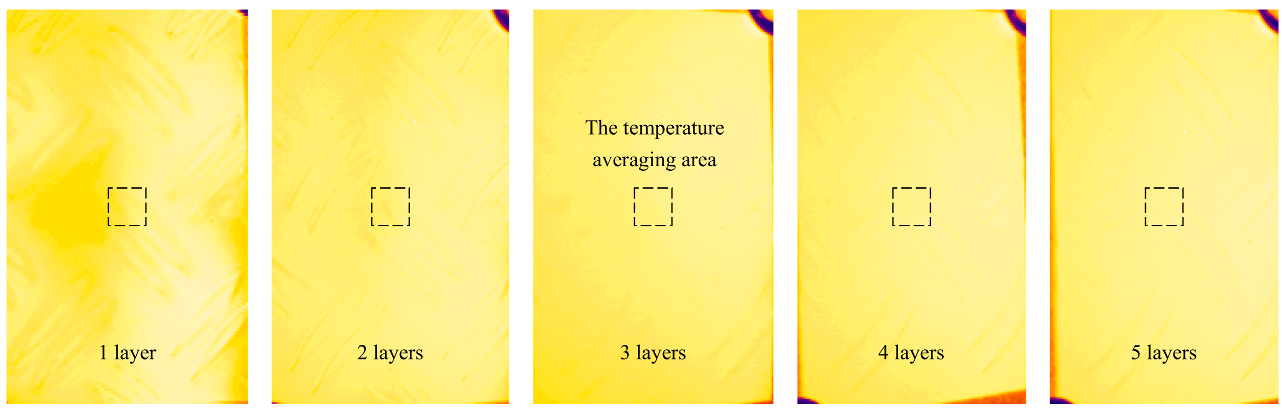

Fig. 5. The thermograms of the plate with different paint layer numbers.

The temperature pattern of the heated aluminum plate surface was captured using a thermo imager [39]. To correctly measure the temperature with the thermal imager, Testo 882 (accuracy ±2 °C) was necessary to set the emissivity E of the examined surface [40]. The emissivity depends on the material and surface treatment; for example, it was 0.1 for polished aluminum and 0.3 for matte [41]. To eliminate the emissivity variation over the surface, the upper surface of the plate was uniformly coated with a black matte paint Bosny flat black No. 4. Depending on the number of coated layers, the emissivity of the black paint ranges from 0.9 to 1.0. Therefore, the required number of coating layers and emissivity of the resulting coating must be determined experimentally (Fig. 4). The aluminum plate with a painted top was set on a heat-insulating material base. A thermocouple was attached to the lower side in the center of the plate, and thermocouple's junction (bead) was 0.5 mm deep inside the plate. The center plate temperature was recorded over time using the data acquisition system. Before each measurement, one layer of the spray paint was added and dried for 3 h. The prepared plate was installed on the test rig and heated by a vertical air flow at 150 °C. When the steady state was reached, the temperature trend was recorded in a log file. In this state, thermograms of the surface were recorded up to five times with an interval of 5–10 s. The time of measurement was saved in the thermogram file properties. The plate temperature was determined on the thermogram and from the log file at the same moment. In the thermogram, the local temperature of the plate was averaged over the area around the junction of thermocouple (Fig. 4b). Temperature data were averaged over five measurements. The corrected emissivity is calculated based on the Stefan-Boltzmann law:

$$E = E_0 \left(\frac{t_{TI} + 273.15}{t_{TC} + 273.15} \right)^4,$$

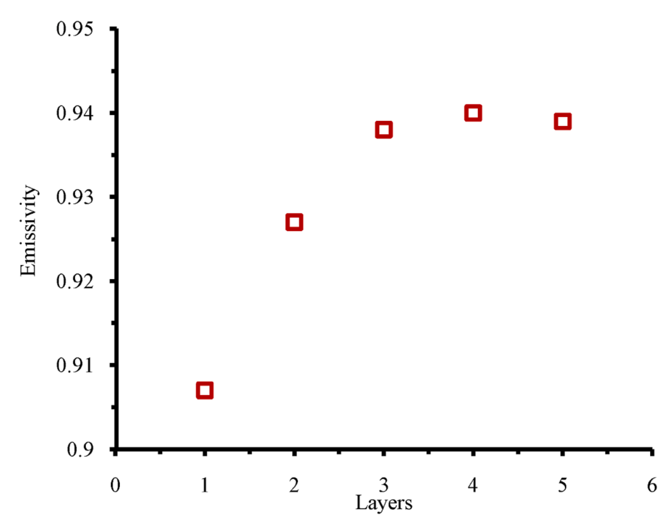

Fig. 6. The plate emissivity various with paint layer numbers.

where E_0 is the emissivity configured in the thermal imager, t_{TI} is the temperature measured by the thermal imager, t_{TC} is the temperature measured by the thermocouple.

Fig. 5 shows the change in the temperature patterns with an increase in the number of coated layers. It can be seen that in the measurement area, the temperature field stabilized after four paint cost. The calculation results (Fig. 6) show that the emissivity stabilizes after four layers as well. As a result, the emissivity of the thermo imager was configured to 0.94±0.01(0.95) in the following experiments, using the five-layer

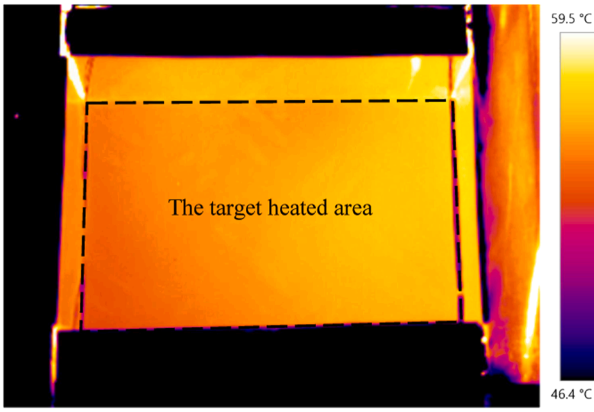

Fig. 7. The example of the thermogram, saved as a jpg file.

Table 2
The ranges of relative uncertainty of measured values.

Calculated quantity	Uncertainty range,%	
	PUF-20	PUF-80
Fiber diameter	2.92	4.58
Flow rate	0.40–2.47	0.61–9.48
Inlet temperature	0.17–0.34	0.11–0.21
Outlet temperature	0.10–0.14	0.18–0.21
Wall temperature	2.23–2.23	2.56–3.90
Pressure drop	1.17–8.94	0.58– 11.01

coating of the plate.

The following procedure was used to study heat transfer from the heated wall. With the autotransformer, the required air flow was set and maintained in the range from 5 to 60 m3 h^{-1}. The aluminum plate's surface temperature was set at 60–75 °C after the heat gun's height was adapted. The sensor data were continuously recorded using the data acquisition system. The temperatures of the air and the plates stabilized after 10–30 min, and the thermogram of the latter was taken with the thermal imager five times with an interval of 10–30 s. In both the longitudinal and cross directions, an imager's objective could be pointed at the plate's normal at an angle between 10 and 20°. To maximize coverage of the "heated window" area, the distance between the objective and the measurement area was adjusted. The shooting moments were saved in the thermogram file properties. The recorded data from the acquisition system and the data from the thermal imager were time-synchronized during the subsequent calculations.

To determine the average surface temperature of the plate, the thermogram's data were exported to a spreadsheet program. Each thermogram consisted of an array of 320 by 240 points (the resolution of the thermal imager matrix in pixels). In this case, the thermogram included both the target heating area of the plate and a small "parasitic" space surrounding it (Fig. 7). Using a procedure (macro) specially developed for the spreadsheet processor, the cells containing the temperature of the target area were selected (the dashed polygon). The area-average temperature is calculated as the arithmetic mean of the selected cells.

When measuring the pressure drop, no heating was used and the air temperature at the inlet was 25–30 °C. The air flow rate was smoothly increased by 2 m^3 h^{-1} increments from 2 to 80 m^3 h^{-1}, and the pressure drop at the inlet and outlet of the sample was measured.

Uncertainty analysis of the measured and calculated quantities was performed according to well-known procedures [38,42]. The ranges of relative uncertainty for the measured values are shown in Table 2, and those for the calculated values are given in Table 6.

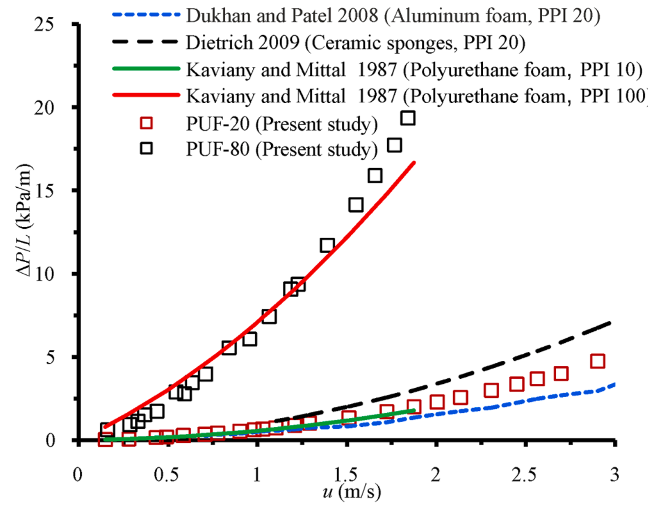

Fig. 8. The pressure gradient as a function of velocity.

Table 3
The experimentally determined b_1 and b_2 coefficients in Eq. (1).

Tested samples	b_1	b_2
PUF-20	99	533
PUF-80	2443	4315

3. Results and discussion

3.1. Pressure drop and friction factor

The pressure drop is plotted against flow velocity in Fig. 8. The data from authors are provided for the metal and PUF for comparison. The pressure drop of the PUF-20 sample was compared with the experimental data obtained by Dukhan and Patel [25], Dietrich et al. [26] and Kaviani and Mittal [33] for PPIs of 20, 20 and 10 respectively. The experimental data of Kaviani and Mittal [33] at PPI 100 were used for comparison with the PUF-80 sample.

Fig. 8 demonstrates that an increase in PPI causes an increase in the pressure drop of PUF, similar to MF. The increase in the pressure drop was associated with an increase in the specific surface area of the foam. For the PUF-20 sample, the pressure drop was in better agreement with Kaviani and Mittal [33] because they tested PUF with a porosity of 0.98, similar to our study. When PUF-20 was compared with the MF at PPI 20, our data were in better agreement with the data obtained by Dukhan and Patel [25] at a lower velocity, and with increasing velocity, the pressure drop of PUF increased faster than that of the MF. When comparing a sample of PUF-20 with Dietrich et al. [26], the pressure drop was higher, since the pressure drop had been obtained for the porosity of 0.85, which was lower than that in our study. The pressure drop of the PUF-80 sample was also in better agreement with the experimental data of Kaviani and Mittal [33] at PPI 100 obtained for PUF.

The measured pressure drop of each sample can be described with the polynomial as follows:

$$\frac{\Delta P}{L} = b_1 u + b_2 u^2, \quad (1)$$

where b_1 and b_2 are fitting curve coefficients (coefficients of determination are no less than 0.99) given in table 3, $u = u_0\,\varepsilon^{-1}$ is the velocity in the PUF, ε is the foam porosity, u_0 is the average velocity in the channel, $\Delta P\,L^{-1}$ is the pressure gradient.

To predict the pressure drop in MF, many authors derive a correlation for the friction factor f as a function of the Reynolds number Re [28], similar to the pressure drop in a pipe. In the present study, the

Table 4
The experimentally determined *A* and *B* coefficients by equations (5).

Tested samples	*A*	*B*
PUF-20	0.766	0.246
PUF-80	0.955	0.439

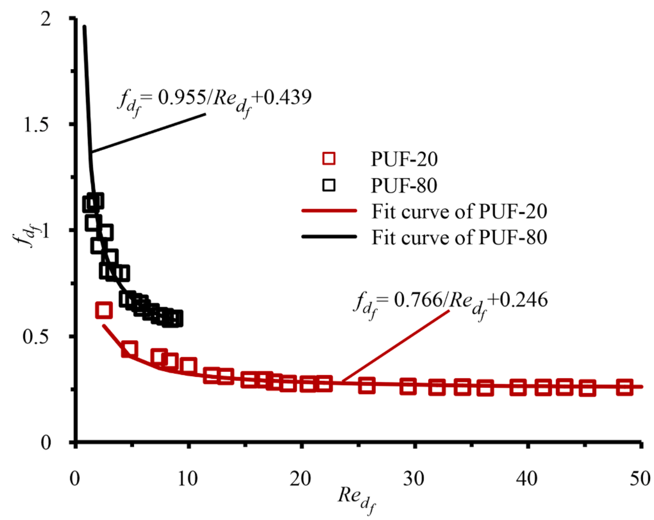

Fig. 9. The friction factor as a function of the fiber diameter based Reynolds number.

friction factor based on the fiber diameter is defined as:

$$f_{d_f} = \frac{A}{\mathrm{Re}_{d_f}} + B, \tag{2}$$

where A and B are experimental coefficients.

The based on the fiber diameter Reynolds number is:

$$\mathrm{Re}_{d_f} = \frac{\rho d_f u}{\mu}, \tag{3}$$

where d_f is the fiber diameter, μ is air viscosity.

The pressure drop is defined according to the Darcy-Weisbach equation:

$$\frac{\Delta P}{L} = f_{d_f} \cdot \frac{\rho u^2}{d_f 2} = \left(\frac{A}{\mathrm{Re}_{d_f}} + B\right) \frac{\rho u^2}{d_f 2} = \frac{A}{\frac{2d_f^2}{\mu}} u + \frac{d_f}{\rho b_2} u^2, \tag{4}$$

Combining Eqs. (1) and (4), the A and B coefficients (table 4) are calculated as follows:

$$A = \frac{b_1 2 d_f^2}{\mu}, \ B = \frac{d_f}{\rho b_2}. \tag{5}$$

Fig. 9 shows good agreement between the friction coefficient correlation (2) and the experimental values; the maximum deviations for PUF-20 and PUF-80 were 15% and 18%, respectively, and the average deviations were 4% and 5%, respectively. The based on the fiber diameter friction factor for the PUF-80 sample is higher than the PUF-20 sample due to the greater pressure drop.

The Darcy-Forchheimer equation is also widely used to describe the pressure drop in open cell foams [28]:

$$\frac{\Delta P}{L} = \frac{\mu}{K} u + \rho \frac{F}{\sqrt{K}} u^2, \tag{6}$$

where K is the permeability of the porous medium and F is Forchheimer coefficient are calculated as follows:

Table 5
The experimentally determined permeability *K* and Forchheimer *F* coefficients.

Tested samples	*K*	*F*
PUF-20	1.889×10^{-7}	0.198
PUF-80	7.535×10^{-9}	0.318

Table 6
The ranges of relative uncertainty of calculated values.

Calculated quantity	Uncertainty range,%	
	PUF-20	PUF-80
Re_{d_f}	2.96–3.83	4.62–10.53
f	3.57–10.63	4.78–19.86
K	1.85–9.28	0.84–10.19
F	2.05–10.22	1.35–19.33
Re_K	1.05–5.26	0.74–10.76
Overall HTC	6.58–8.47	9.23–12.34
Nu_{d_f}	7.20–8.96	10.30– 13.16
Nu_K	6.65–9.66	9.24–13.35
Colburn *j* factor	6.73–11.00	9.26–17.15
TPF	7.17–9.19	9.36–14.00

$$K = \frac{\mu}{b_1}, \tag{7}$$

$$F = \frac{b_2 \sqrt{K}}{\rho}. \tag{8}$$

The experimental friction factor based on the permeability is calculated as follows:

$$f_K = \frac{\Delta P}{L} \cdot \frac{\sqrt{K}}{\rho u^2}. \tag{9}$$

The friction factor correlation based on the permeability is defined as follows:

$$f_K = \frac{1}{\mathrm{Re}_K} + F, \tag{10}$$

where the Reynolds number based on the permeability is defined as follows:

$$\mathrm{Re}_K = \frac{\rho \sqrt{K} u}{\mu}. \tag{11}$$

The permeability and Forchheimer coefficient values for each foam are listed in table 5. Fig. 10 compares the correlations obtained in this study and other researchers. The friction factor predicted by the correlation (10) agrees well with the experimental data, the maximum and average deviation was 18% and 5% respectively, that similar to correlation (2). The friction factor at the same Reynolds number varies only slightly between authors. The friction factor was in better agreement with Kaviany and Mittal [33] as they also tested PUF. From minimum to maximum Re_K the friction factor predicted by Paek et al. [27] for aluminum foam was 1.26 to 1.75 times lower than the friction factor of the current work. The friction factor predicted by Wang and Guo [28] for stainless steel foams was lower than the current study by a factor of 5. The significant differences from Wang and Guo [28] can be explained by the fact that in their work, the pressure drop was determined at velocity ranging from 7 to 26 m s^{-1}. The current work was performed at velocities ranging from 0.1 to 3 m s^{-1}. Wang and Guo [28] pointed out that the permeability and Forchheimer coefficient are dependent on the velocity range. On the other hand, the difference in ligament structures of metal and PUF can lead to differences in pressure drop and friction factor, and it should be noted that the friction factor of MF can also differ significantly depending on the manufacturing process.

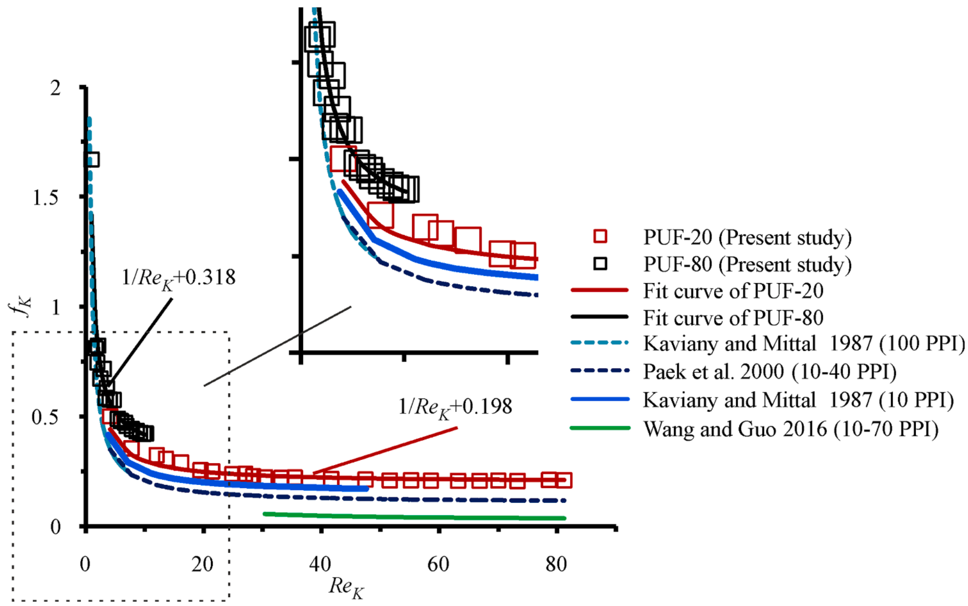

Fig. 10. The friction factor as a function of the permeability based Reynolds number.

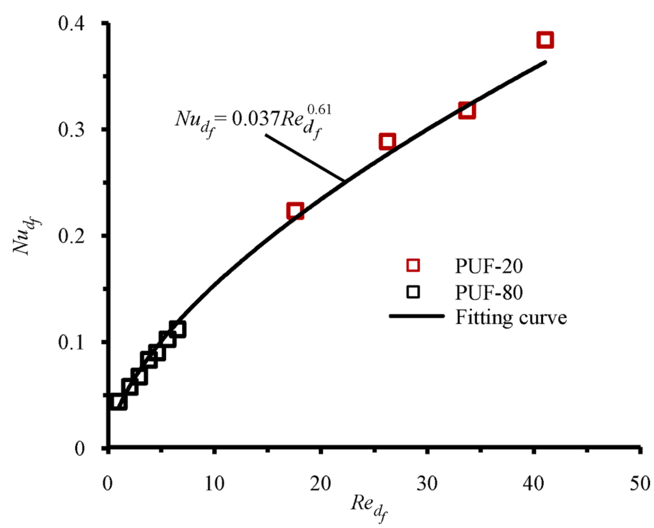

Fig. 11. The Nusselt number as a function of Reynolds number, reference dimension is the fiber diameter.

3.2. Heat transfer

The overall HTC of the channel with foam inserts is defined as follows:

$$\mathrm{HTC} = \frac{Q}{A_{wall} \cdot \Delta T} \tag{12}$$

where ΔT is the difference between the mean wall temperature T_{wall} and the mean flow temperature T_{flow} in the foam, A_{wall} is the area of the aluminum heated wall. The mean flow temperature T_{flow} is calculated by the following equation:

$$T_{flow} = \frac{T_{inlet} + T_{outlet}}{2} \tag{13}$$

where T_{inlet}, T_{outlet} are the inlet and outlet temperature of the test section. The heat flow rate Q is defined as:

$$Q = \dot{m} \cdot c_p \cdot (T_{outlet} - T_{inlet}) \tag{14}$$

where $\dot{m}$, c_p are the mass flow rate and the heat capacity of the air respectively.

For the channel with foam insert the Nusselt number based on fiber diameter is defined by:

$$Nu_{d_f} = \frac{\mathrm{HTC} \cdot d_f}{k_f} \tag{15}$$

where k_f the thermal conductivity of the air.

As the Reynolds number based on the fiber diameter increases, the Nusselt number also increases (Fig. 11). The differences in the Reynolds number of the studied samples are associated with differences in the fiber diameters (table 1). Since the PUF-20 sample had a larger fiber diameter, the maximum Nusselt number was observed for the PUF-20 sample. The minimum Nusselt number with foam inserts was 0.04, and the maximum was 0.4. The following correlation was obtained for the Nusselt number as a function of the Reynolds number based on fiber the diameter:

$$Nu_{d_f} = 0.037\mathrm{Re}_{d_f}^{0.61} \tag{16}$$

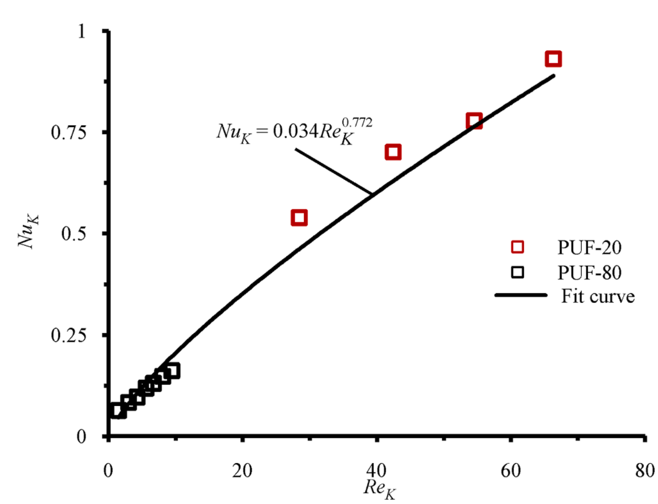

Fig. 12. The Nusselt number as a function of Reynolds number, reference dimension is the permeability.

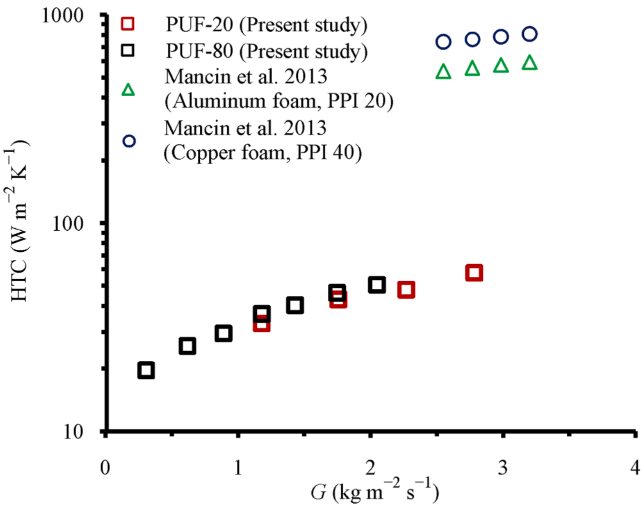

Fig. 13. The overall HTC as a function of the mass velocity.

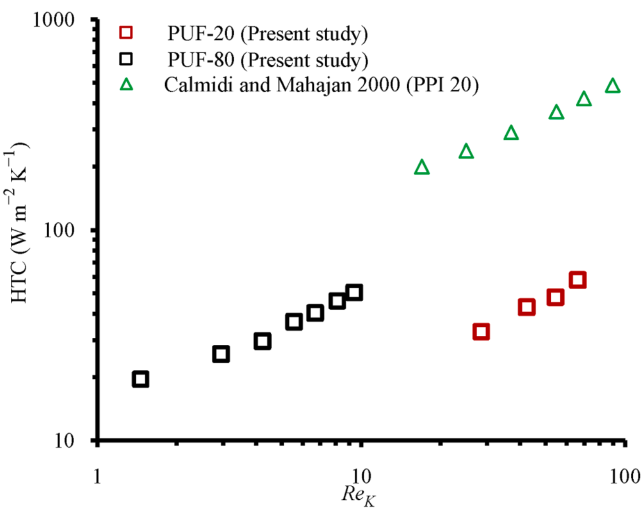

Fig. 14. The overall HTC as function of the permeability based Reynolds number.

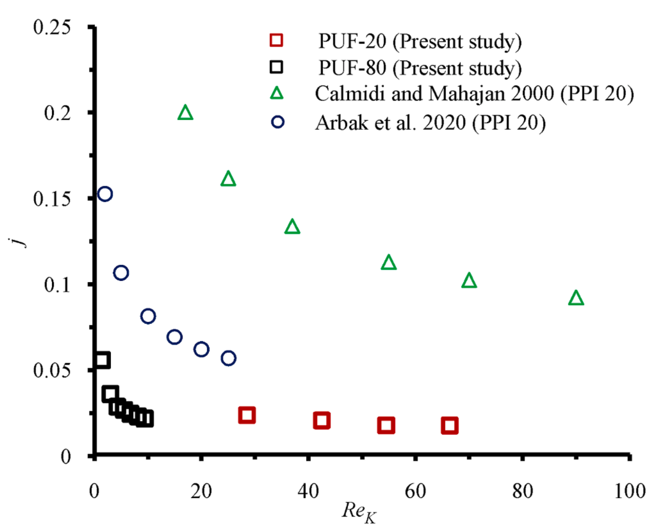

Fig. 15. The Colburn j factor as function of the Reynolds number, reference dimension is the permeability.

From Fig. 11 is clear that the Nusselt number based on the fiber diameter is independent from PUF pore density. The Nusselt number as a function of the Reynolds number for PUF-20 and PUF-80 was well described by a single correlation. Also, it suggests that the fiber diameter is suitable as a characteristic length for PUF. The power law with the Reynolds number exponent is 0.61, which coincides with the obtained Arbach and Doohan [22] exponent in the power law equation for the MF. Therefore, the effect of the Reynolds number on the heat transfer in the PUF was similar with the MF. However, the constant in the power law equation obtained by Arbach and Doohan [22] is equal to 0.36, because of much higher overall HTC in the MF.

The Nusselt number based on permeability is defined by:

$$Nu_K = \frac{\mathrm{HTC}\cdot\sqrt{K}}{k_f} \tag{17}$$

Fig. 12 shows the Nusselt number as a function of permeability Reynolds number. The following correlation is obtained for the Nusselt number as a function of Reynolds number based on the fiber diameter:

$$Nu_K = 0.034\mathrm{Re}_K^{0.772} \tag{18}$$

The Nusselt number based on the permeability Reynolds number for PUF-20 and PUF-80 can be described by a single correlation similar to the fiber diameter based Reynolds number Eq. (16)). However, the correlation based on the fiber diameter was in better agreement with experimental data, the average deviations for Eqs. (16) and ((18) were 5% and 16%, respectively. On the other hand, advantage of Eq. (18) is that it does not require the measurement of the fiber diameter.

In Fig. 13, the overall HTC obtained in the present study is compared with the results of Mancin et al. [12] for aluminum and copper foam with PPI 20. For minimal and maximal mass velocities, the HTC of PUF was 20 and 64 W m^{-2} K^{-1}, respectively. As seen, the overall HTC of PUF was much lower than that of MF. The overall HTC of aluminum and copper foams exceeds the overall HTC of PUF by factors of 9.5 and 12, respectively. For comparison with the data of Calmidi et al. [15], in Fig. 14, the overall HTC is presented in relation to the based on permeability Reynolds number. The aluminum foam with a PPI of 20 had an overall HTC seven times greater than that of PUF. Although the Reynolds number for the PUF-80 sample was less than that of PUF-20, the HTC of the two PUF samples at the same mass velocities were almost identical. Edouard et al. [32] also investigated the overall HTC of PUF in an air flow. According to their study, the overall HTC varied from 100 to 120 W m^{-2} K^{-1} for air velocities in the range from 0.018 to 0.32 m s^{-1}, i.e. almost independent of velocity. The overall HTC obtained in our study differed from the data of Edouard et al. [32] by two and five times for the maximum and minimum flow rates, respectively. The greater difference at the minimal velocity was associated with large uncertainties, which can be confirmed by the fact that in Edouard et al. [32], the flow velocity did not affect the HTC.

The difference between PUF and MF for the overall HTC was greater for the copper foam, since copper has a higher thermal conductivity. The ratio of thermal conductivity of fluid and solid k_f/k_s was 1.37 $\times$ 10^{-1}, 1.1 $\times$ 10^{-4} and 6.7 $\times$ 10^{-5} for PUF, aluminum and copper foam, respectively. The thermal conductivity of the copper foam was higher than that of PUF foam by two to three orders of magnitude. The low value of the thermal conductivity of the PUF foam material leads to a significant decrease in the HTC in the channel with PUF inserts compared with MF. The low thermal conductivity of foams increases the thermal resistance of the solid phase, which limits the heat transfer along the foam ligaments from the heated wall to the flow. It should be noted that the data obtained in the present study are not consistent with those of the analytical studies by Lu et al. [30] and Xu et al. [31]. The results of the analytical study showed that with an increase in k_f/k_s from 1 $\times$ 10^{-5} to 1 $\times$ 10^{-1}, the Nusselt number decreased by two orders of magnitude, but in the present study, the HTC decreased by one order of magnitude (by a factor of 12) when comparing PUF with MF Mancin

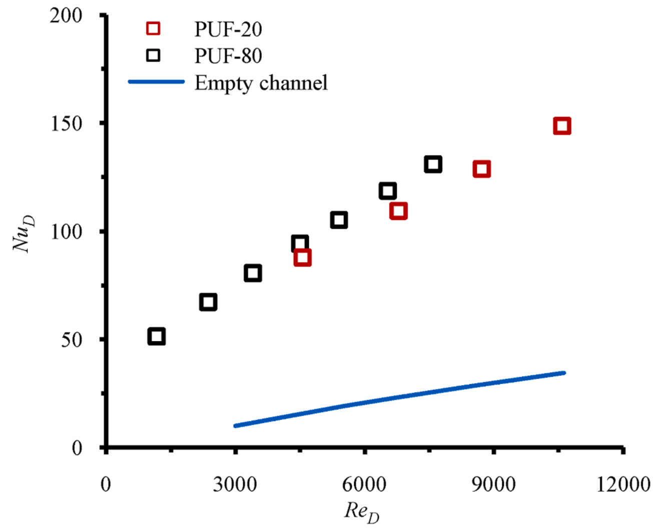

Fig. 16. The Nusselt number as a function of Reynolds number, reference dimension is the hydraulic diameter of the channel.

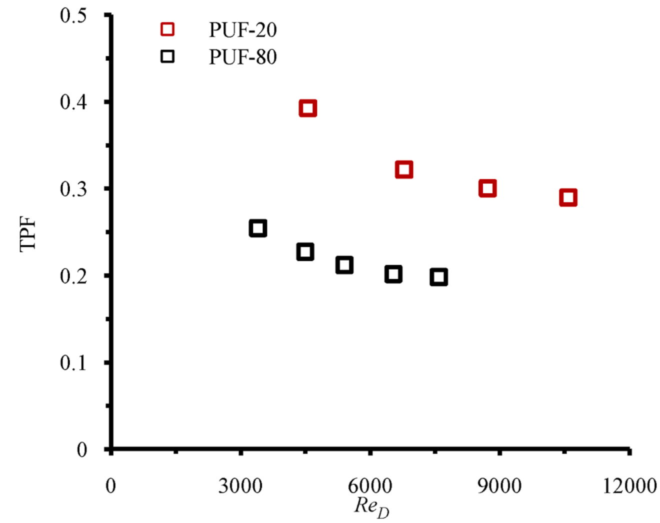

Fig. 17. The TPF as a function of the Reynolds number, reference dimension is the hydraulic diameter of the channel.

et al. [12]. However, an experimental study by Kouidr and Madani [16] demonstrated that the Nusselt number decreased by a factor of 1.6 as k_f/k_s increased by one order of magnitude. In their case, MF with different thermal conductivities and water as the working medium was used. The analytical models presented by Lu et al. [30] and Xu et al. [31] were verified on MF, which is possibly the reason why their data are not consistent with our data.

Representing the Colburn j factor as a function of the Reynolds number is one way to calculate the performance of heat transfer [22]. The Colburn factor is defined as follows:

$$j = St\mathrm{Pr}^{2/3}, \tag{19}$$

where Pr is the Prandtl number. The Stanton number St is defined as:

$$St = \frac{Nu_K}{\mathrm{Re}_K\mathrm{Pr}}, \tag{20}$$

The Colburn factor j as a function of the permeability Reynolds number for the PUF and MF is shown in Fig. 15. With an increase in the Reynolds number, the Colburn factor decreased, similar to Calmidi et al. and Abrak et al., while its values for PUF were significantly lower than those for MF. However, the values are closer to the data of Abrak et al., since they studied the heat exchange in aluminum foam with water at a ratio k_f/k_s of 2.5×10^{-3}. Fig. 15 also shows that the j factor is higher for the PUF-80 sample due to the lower values of the permeability based Reynolds number. The maximum values for the PUF-20 and PUF-80 samples were 0.06 and 0.024, respectively.

Fig. 16 shows the Nusselt number Nu_D based on the channel hydraulic diameter with a PUF and an empty channel for comparison. The Nusselt number of the empty channel Nu_D^0 is calculated using the empirical correlation for the Reynolds number Re_D based on the channel hydraulic diameter $Re_D > 3000$ using the Gnielinski equation [43]:

$$Nu_D^0 = \frac{(f_D^0/8)\mathrm{Re}_D\mathrm{Pr}}{1.07 + 12.7(f_D^0/8)^{0.5}\left(\mathrm{Pr}^{2/3} - 1\right)}, \tag{21}$$

where f_D^0 is the friction factor of the empty channel calculated using the Blasius equation for Reynolds number ($3000 < Re_D < 20{,}000$) [21]:

$$f_D^0 = 0.3164\mathrm{Re}_D^{0.25}. \tag{22}$$

The Reynolds number based on the channel hydraulic diameter is defined as:

$$\mathrm{Re}_D = \frac{\rho u D}{\mu}, \tag{23}$$

where D is the hydraulic diameter of the channel.

The Nusselt number of PUF based on the channel hydraulic diameter is defined as:

$$Nu_D = \frac{\mathrm{HTC}\cdot D}{k_f}, \tag{24}$$

The Nu_D for the channel with PUF was noticeably higher than that of the empty channel (Fig. 16), despite the fact that the HTC of PUF was significantly lower than that of MF (Figs. 13 and 14). The heat transfer intensification in the channel with all tested PUF can be explained by the intensive mixing of the flow passing through the complex structure of the foams. At the same Re_D, the heat transfer intensity was slightly higher for foams with lower PPI.

To estimate the heat transfer enhancement at equal pumping power, the following equation of the thermal performance factor TPF is employed [21]:

$$\mathrm{TPF} = \frac{Nu_D/Nu_D^0}{\left(f_D/f_D^0\right)^{1/3}}, \tag{25}$$

where f_D is the frication factor of PUF based on the hydraulic diameter is defined as:

$$f_D = \frac{\Delta P}{L}\frac{2D}{\rho u^2}, \tag{26}$$

Fig. 17 shows TPF of the PUF for various Reynolds numbers. As can be seen for both tested PUF, the TPF value is less than 1, which means that at equal pumping power, the HTC of PUF is less than that of the empty channel. Although both PUF have similar HTC values, the TPF was higher for the PUF-20 foam because PUF-80 foam had a higher friction factor. This indicates that PUF with a lower PPI is more suitable as a heat transfer enhancer. The maximum value of the TPF is 0.37 and 0.24 for PUF-20 and PUF-80, respectively, at the lowest Reynolds number. As the Reynolds number increased, the TPF decreased. Huang et al. [21] also showed a decrease in TPF with an increasing Reynolds number for MF. However, the TPF was above 1 for Reynolds number of less than 3000. The best TPF of the MF is due to the high thermal conductivity of the metal. Although the pressure drop in MF is close to that in PUF, the HTC of MF can be higher by a factor of 12 due to the high thermal conductivity.

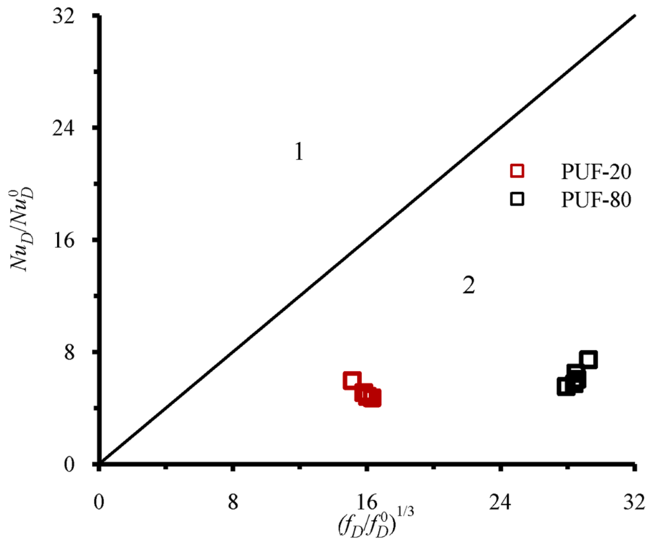

Fig. 18. The Nusselt number ratio as a function of the friction factor ratio.

Fig. 18 shows the diagram divided into two regions for the Nusselt number and friction factor ratios. The first region is on the left with respect to the diagonal, corresponding to the value of the TPF > 1, and the second region is on the right, corresponding to TPF < 1. Thermo hydraulically efficient heat transfer intensifiers must fall into the first region. As can be seen, the PUF is in the second region, that is, the pumping costs exceed the effect of heat transfer intensification. Despite the increases in friction factors of 17 and 30 times for PUF-20 and PUF-80, respectively, the use of the above foams intensified the heat transfer by six and seven times, respectively.

Although the heat transfer of PUF is an order of magnitude less than that of MF, the results of the experimental analysis show that inserts with PUF also significantly intensify the heat transfer compared to an empty channel. However, due to the additional pressure drop due to turbulence, the increase in the friction factor exceeded the increase in heat transfer enhancement. Despite this, PUF can still be used when the compactness or mass of the heat exchanger is more important than pumping costs. When comparing MF and PUF, it is important to note that MF will require less volume to achieve the same heat rate due to its higher HTC, based on its thermo physical properties. On the other hand, PUF are lighter and less expensive than MF.

4. Conclusion

The experimental study of the hydraulic and heat transfer characteristics of a rectangular channel filled with polyurethane foam (PUF) inserts with a thermal conductivity of 0.2 $W \cdot m^{-1} \cdot K^{-1}$ in the air flow was carried out. The pressure drop through PUF is similar to that of MF at the same pore density and porosity. The correlation coefficients for the friction factor based on the permeability Reynolds number are closer at different pore densities tested for PUF, compared to correlations obtained for fiber diameter based Reynolds number. This shows that permeability based Reynolds number is less dependent on the pore density; therefore, it is better to use as a characteristic length to determine the friction factor in the foam. The Nusselt number as a function of the Reynolds number based on the fiber diameter is independent of the PUF pore density and can be described by the correlation for different pore densities. The intensity of the heat transfer from the wall of the channel filled with PUF was 6–7 times higher than that of the empty channel. In this case, the thermal performance factor was in the range of 0.3 to 0.4. Mainly due to the lower thermal conductivity of polyurethane, PUF foams have a 7–12 times lower overall HTC compared to MF. It should be noted that some differences between PUF and MF can also be caused by the higher porosity, strut surface, etc. However PUF are lighter and less expensive than MF. Therefore the mass and cost of the heat exchanger is important, PUF can be used instead of MF.

CRediT authorship contribution statement

Aidar Hayrullin: Conceptualization, Investigation, Writing – review & editing, Writing – original draft. **Alex Sinyavin:** Data curation, Writing – review & editing. **Aigul Haibullina:** Visualization, Methodology. **Vladimir Ilyin:** Supervision, Project administration.

Declaration of Competing Interest

The authors declare that they have no known competing financial interests or personal relationships that could have appeared to influence the work reported in this paper.

Data Availability

Data will be made available on request.

Acknowledgments

We would like to acknowledge financial supports for this work provided by the Russian Science Foundation, grant number 21–79–10406, https://rscf.ru/en/project/21–79–10406/ accessed on 15 September 2023.

References

[1] A.M. Bayomy, M.Z. Saghir, Heat transfer characteristics of aluminum metal foam subjected to a pulsating/steady water flow: experimental and numerical approach, Int. J. Heat Mass Transf. 97 (2016) 318–336, https://doi.org/10.1016/j.ijheatmasstransfer.2016.02.009.

[2] S. De Schampheleire, P. De Jaeger, H. Huisseune, B. Ameel, C. T'Joen, K. De Kerpel, M. De Paepe, Thermal hydraulic performance of 10 PPI aluminium foam as alternative for louvered fins in an HVAC heat exchanger, Appl. Therm. Eng. 51 (2013) 371–382, https://doi.org/10.1016/j.applthermaleng.2012.09.027.

[3] A.A. Hmad, N. Dukhan, Cooling sesign for PEM fuel-cell stacks employing air and metal foam: simulation and experiment, Energies 14 (2021) 2687, https://doi.org/10.3390/en14092687.

[4] A. Mustaffar, D. Reay, A. Harvey, The melting of salt hydrate phase change material in an irregular metal foam for the application of traction transient cooling, Therm. Sci. Eng. Progr. 5 (2018) 454–465, https://doi.org/10.1016/j.tsep.2018.02.001.

[5] C. Welsford, A.M. Bayomy, M.Z. Saghir, Role of metallic foam in heat storage in the presence of nanofluid and microencapsulated phase change material, Therm. Sci. Eng. Progr. 7 (2018) 61–69, https://doi.org/10.1016/j.tsep.2018.05.003.

[6] S.A. Solovev, O.V. Soloveva, I.G. Akhmetova, Y.V. Vankov, D.L. Paluku, Numerical simulation of heat and mass transfer in an open-cell foam catalyst on example of the acetylene hydrogenation reaction, ChemEngineering 6 (2022) 11, https://doi.org/10.3390/chemengineering6010011.

[7] Y. Li, S. Wang, Y. Fu, Y. Zhao, L. Yue, Influence of foamed metal core flow heat transfer enhancement on the performance of thermoelectric generators with different power generation characteristics, Therm. Sci.Eng. Progr. 31 (2022), 101300, https://doi.org/10.1016/j.tsep.2022.101300.

[8] H. Wang, L. Guo, K. Chen, Theoretical and experimental advances on heat transfer and flow characteristics of metal foams, Sci. China Technol. Sci. 63 (2020) 705–718, https://doi.org/10.1007/s11431-019-1455-0.

[9] S. Mancin, C. Zilio, A. Cavallini, L. Rossetto, Heat transfer during air flow in aluminum foams, Int. J. Heat Mass Transf. 53 (2010) 4976–4984, https://doi.org/10.1016/j.ijheatmasstransfer.2010.05.033.

[10] S. Mancin, C. Zilio, L. Rossetto, A. Cavallini, Heat transfer performance of aluminum foams, J. Heat Transfer 133 (2011), 060904, https://doi.org/10.1115/1.4003451.

[11] S. Mancin, C. Zilio, L. Rossetto, A. Cavallini, Foam height effects on heat transfer performance of 20 ppi aluminum foams, Appl. Therm. Eng. 49 (2012) 55–60, https://doi.org/10.1016/j.applthermaleng.2011.05.015.

[12] S. Mancin, C. Zilio, A. Diani, L. Rossetto, Air forced convection through metal foams: experimental results and modeling, Int. J. Heat Mass Transf. 62 (2013) 112–123, https://doi.org/10.1016/j.ijheatmasstransfer.2013.02.050.

[13] F.Ç. Durmus, L.P. Maiorano, J.M. Molina, Open-cell aluminum foams with bimodal pore size distributions for emerging thermal management applications, Int. J. Heat Mass Transf. 191 (2022), 122852, https://doi.org/10.1016/j.ijheatmasstransfer.2022.122852.

[14] M. Sun, G. Yan, M. Ning, C. Hu, J. Zhao, F. Duan, D. Tang, Y. Song, Forced convection heat transfer: a comparison between open-cell metal foams and additive manufactured kelvin cells, Int. Commun. Heat Mass Transf. 138 (2022), 106407, https://doi.org/10.1016/j.icheatmasstransfer.2022.106407.

[15] V.V. Calmidi, R.L. Mahajan, Forced convection in high porosity metal foams, J. Heat Transf. 122 (2000) 557–565, https://doi.org/10.1115/1.1287793.

[16] A. Kouidri, B. Madani, Experimental study of forced convection through various metallic foam samples: effect of effective thermal conductivity on Nusselt correlation, J. Therm. Anal. Calorim. (2022), https://doi.org/10.1007/s10973-022-11779-6.

[17] A. Hamadouche, R. Nebbali, H. Benahmed, A. Kouidri, A. Bousri, Experimental investigation of convective heat transfer in an open-cell aluminum foams, Exp. Therm. Fluid Sci. 71 (2016) 86–94, https://doi.org/10.1016/j.expthermflusci.2015.10.009.

[18] J.-J. Hwang, G.-J. Hwang, R.-H. Yeh, C.-H. Chao, Measurement of interstitial convective heat transfer and frictional drag for flow across metal foams, J. Heat Transf. 124 (2002) 120–129, https://doi.org/10.1115/1.1416690.

[19] J.-S. Noh, K.B. Lee, C.G. Lee, Pressure loss and forced convective heat transfer in an annulus filled with aluminum foam, Int. Commun. Heat Mass Transf. 33 (2006) 434–444, https://doi.org/10.1016/j.icheatmasstransfer.2005.11.003.

[20] C. Hutter, D. Büchi, V. Zuber, Ph. Rudolf von Rohr, Heat transfer in metal foams and designed porous media, Chem. Eng. Sci. 66 (2011) 3806–3814, https://doi.org/10.1016/j.ces.2011.05.005.

[21] Z.F. Huang, A. Nakayama, K. Yang, C. Yang, W. Liu, Enhancing heat transfer in the core flow by using porous medium insert in a tube, Int. J. Heat Mass Transf. 53 (2010) 1164–1174, https://doi.org/10.1016/j.ijheatmasstransfer.2009.10.038.

[22] A. Arbak, N. Dukhan, Performance and heat transfer measurements in asymmetrically-heated metal foam cooled by water, Therm. Sci. Eng. Progr. 20 (2020), 100688, https://doi.org/10.1016/j.tsep.2020.100688.

[23] B. Dietrich, Heat transfer coefficients for solid ceramic sponges – experimental results and correlation, Int. J. Heat Mass Transf. 61 (2013) 627–637, https://doi.org/10.1016/j.ijheatmasstransfer.2013.02.019.

[24] S. Xu, Z. Wu, H. Lu, L. Yang, Experimental study of the convective heat transfer and local thermal equilibrium in ceramic foam, Processes 8 (2020) 1490, https://doi.org/10.3390/pr8111490.

[25] N. Dukhan, P. Patel, Equivalent particle diameter and length scale for pressure drop in porous metals, Exp. Therm. Fluid Sci. 32 (2008) 1059–1067, https://doi.org/10.1016/j.expthermflusci.2007.12.001.

[26] B. Dietrich, W. Schabel, M. Kind, H. Martin, Pressure drop measurements of ceramic sponges—Determining the hydraulic diameter, Chem. Eng. Sci. 64 (2009) 3633–3640, https://doi.org/10.1016/j.ces.2009.05.005.

[27] J.W. Paek, B.H. Kang, S.Y. Kim, J.M. Hyun, Effective thermal conductivity and permeability of aluminum foam materials1, Int. J. Thermophys. 21 (2000) 453–464, https://doi.org/10.1023/A:1006643815323.

[28] H. Wang, L. Guo, Experimental investigation on pressure drop and heat transfer in metal foam filled tubes under convective boundary condition, Chem. Eng. Sci. 155 (2016) 438–448, https://doi.org/10.1016/j.ces.2016.08.031.

[29] H. Wang, L. Guo, Volumetric Convective Heat Transfer Coefficient Model for Metal Foams, Heat Transfer Engineering 40 (2019) 464–475, https://doi.org/10.1080/01457632.2018.1432045.

[30] W. Lu, C.Y. Zhao, S.A. Tassou, Thermal analysis on metal-foam filled heat exchangers. Part I: metal-foam filled pipes, Int. J. Heat Mass Transf. 49 (2006) 2751–2761, https://doi.org/10.1016/j.ijheatmasstransfer.2005.12.012.

[31] H.J. Xu, L. Gong, C.Y. Zhao, Y.H. Yang, Z.G. Xu, Analytical considerations of local thermal non-equilibrium conditions for thermal transport in metal foams, Int. J. Therm. Sci. 95 (2015) 73–87, https://doi.org/10.1016/j.ijthermalsci.2015.04.007.

[32] D. Edouard, T. Truong Huu, C. Pham Huu, F. Luck, D. Schweich, The effective thermal properties of solid foam beds: experimental and estimated temperature profiles, Int. J. Heat Mass Transf. 53 (2010) 3807–3816, https://doi.org/10.1016/j.ijheatmasstransfer.2010.04.033.

[33] M. Kaviany, M. Mittal, Natural convection heat transfer from a vertical plate to high permeability porous media: an experiment and an approximate solution, Int. J. Heat Mass Transf. 30 (1987) 967–977, https://doi.org/10.1016/0017-9310(87)90015-9.

[34] M.O.R. Siddiqui, D. Sun, Computational analysis of effective thermal conductivity of microencapsulated phase change material coated composite fabrics, J. Compos. Mater. 49 (2015) 2337–2348, https://doi.org/10.1177/0021998314545193.

[35] C. Tseng, M. Yamaguchi, T. Ohmori, Thermal conductivity of polyurethane foams from room temperature to 20K, Cryogenics (Guildf) 37 (1997) 305–312, https://doi.org/10.1016/S0011-2275(97)00023-4.

[36] D.S.W. Pau, C.M. Fleischmann, M.J. Spearpoint, K.Y. Li, Thermophysical properties of polyurethane foams and their melts, Fire Mater. 38 (2014) 433–450, https://doi.org/10.1002/fam.2188.

[37] S. Kalita, P. Sen, D. Sen, S. Das, A.K. Das, B.B. Saha, Experimental study of nucleate pool boiling heat transfer on microporous structured by chemical etching method, Therm. Sci. Eng. Progr. 26 (2021), 101114, https://doi.org/10.1016/j.tsep.2021.101114.

[38] M.E. Nakhchi, Experimental optimization of geometrical parameters on heat transfer and pressure drop inside sinusoidal wavy channels, Therm. Sci. Eng. Progr. 9 (2019) 121–131, https://doi.org/10.1016/j.tsep.2018.11.006.

[39] K. Yogi, M.M. Godase, M. Shetty, S. Krishnan, S.V. Prabhu, Experimental investigation on the local heat transfer with a circular jet impinging on a metal foamed flat plate, Int. J. Heat Mass Transf. 162 (2020), 120405, https://doi.org/10.1016/j.ijheatmasstransfer.2020.120405.

[40] Testo 882 - thermal imager. Instruction manual. https://static-int.testo.com/media/8d/23/55364e9a2ba1/testo-882-Instruction-manual.pdf, 2022 (accessed 10 December 2022)., (n.d.).

[41] C.-D. Wen, I. Mudawar, Experimental investigation of emissivity of aluminum alloys and temperature determination using multispectral radiation thermometry (MRT) algorithms, J. Mater. Eng. Perform. 11 (2002) 551–562, https://doi.org/10.1361/105994902770343818.

[42] R.J. Moffat, Describing the uncertainties in experimental results, Exp. Therm. Fluid Sci. 1 (1988) 3–17, https://doi.org/10.1016/0894-1777(88)90043-X.

[43] Y.A. Cengel, Heat Transfer: A Practical Approach, 2nd Edition, McGraw-Hill, New York, 2002.